HHS Public Access

Author manuscript

Adv Funct Mater. Author manuscript; available in PMC 2022 June 09.

Published in final edited form as:

Adv Funct Mater. 2021 June 9; 31(24): . doi:10.1002/adfm.202010104.

Induction of 4D spatiotemporal geometric transformations in high cell density tissues via shape changing hydrogels

Yu Bin Lee, **Oju Jeon**, **Sang Jin Lee**, **Aixiang Ding**, **Derrick Wells**

Department of Biomedical Engineering, University of Illinois at Chicago, IL 60612, USA

Eben Alsberg

Department of Biomedical Engineering, University of Illinois at Chicago, IL 60612, USA

Departments of Orthopaedics, Pharmacology, and Mechanical & Industrial Engineering, University of Illinois at Chicago, IL 60612, USA

Abstract

Developing and healing tissues begin as a cellular condensation. Spatiotemporal changes in tissue geometry, transformations in the spatial distribution of the cells and extracellular matrix, are essential for its evolution into a functional tissue. 4D materials, 3D materials capable of geometric changes, may have the potential to recreate the aforementioned biological phenomenon. However, most reported 4D materials are non-degradable and/or not biocompatible, which limits their application in regenerative medicine, and to date there are no systems controlling the geometry of high density cellular condensations and differentiation. Here, we describe 4D high cell density tissues based on shape-changing hydrogels. By sequential photocrosslinking of oxidized and methacrylated alginate (OMA) and methacrylated gelatin (GelMA), bi-layered hydrogels presenting controllable geometric changes without any external stimuli were fabricated. Fibroblasts and human adipose-derived stem cells (ASCs) were incorporated at concentrations up to 1.0×10^8 cells/mL to the 4D constructs, and controllable shape changes were achieved in concert with ASCs differentiated down chondrogenic and osteogenic lineages. Bioprinting of the high density cell-laden OMA and GelMA permitted the formation of more complex constructs with defined 4D geometric changes, which may further expand the promise of this approach in regenerative medicine applications.

Graphical Abstract

ealsberg@uic.edu.

Supporting Information

Supporting Information is available from the Wiley Online Library or from the author.

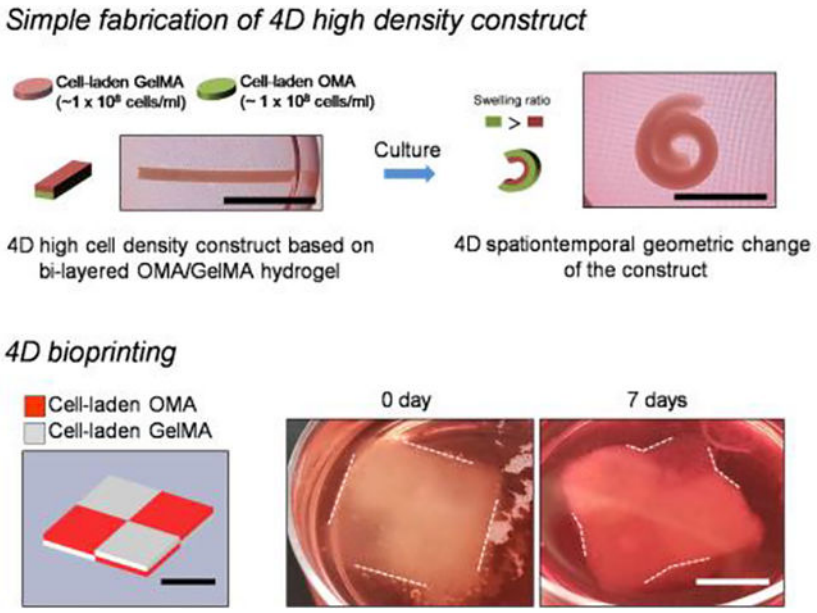

This study reports engineering of 4D high cell density constructs recapitulating the spatiotemporal re-arrangement of native tissues. Bi-layered and bioprinted high cell density constructs (1.0×10^8 cells/mL) with a minimal amount of biodegradable and photocrosslinkable polymers (methacrylated gelatin (GelMA), oxidized and metharcylated alginate (OMA)) enable self-geometric change mediated by higher swelling property of the OMA as compared to GelMA.

Keywords

4D material; High cell density construct; Bioprinting; Stem cell

1. Introduction

Exquisitely controlled temporal changes in cell and extracellular matrix (ECM) arrangement and three-dimensional (3D) geometry play a critical role during tissue and organ morphogenesis, natural healing processes, and performance and maintenance of biologic and physiologic functions.[1, 2] During development and healing, cells often condense into aggregates and then organize themselves and rearrange through processes such as migration and differential cell adhesion to drive the emergence of new or restored cellular spatial placement and tissue geometries.[3] Four-dimensional (4D) materials, which here will be defined as those that undergo controlled temporal changes in geometry in response to specific environmental stimuli, may be valuable in the fields of tissue engineering and regenerative medicine as they could drive or partially recapitulate the aforementioned native geometric changes. In addition, most conventional 3D engineered tissues maintain a defined shape during their formation and may not be able to actively interact in coordination with the geometric changes occurring in surrounding developing or healing tissues. In this respect, the ability to induce defined 4D geometric changes in cytocompatible materials may endow engineered tissues with the capacity to dynamically change their shape in concert with those of neighboring tissues.[4] Since developing and healing tissues often begin as

cellular condensations with minimal ECM, 4D material constructs capable of incorporating high concentrations of cells and enabling extensive cell-cell interactions while still exhibiting tailored geometric shape changes would be valuable in studying and understanding these biological phenomena.[5]

There have been several techniques reported for producing 4D materials and systems for potential use in tissue engineering applications that elicit temporal geometric changes in cell culture conditions. Incorporation of multiple materials or creation of network gradients in a single material have been used to generate spatially varied swelling to exploit it as driving force for the geometric changes. These 4D systems use materials that, for example, swell in response to changes in stimuli such as temperature[6, 7], light [8, 9], or electric fields[10, 11]. However, the non-degradable materials used in the aforementioned stimuli responsive systems have limited cyto- and biocompatibility and/or are unable to provide an environment conducive to cell proliferation, migration, differentiation and ECM production and remodeling. Deformation due to contractility of attached cells on parylene polymer microplates has been exploited to achieve 4D geometric changes,[12] but cells can only be seeded on the surfaces of these plates. There have been several reports of biocompatible 4D hydrogel systems which exhibit the capacity for culture of encapsulate cells and have been engineered to generate spatially differential swelling in cell culture conditions by, for example, attaching two polyethylene glycol (PEG) hydrogel layers with different molecular weights[13], gradient crosslinking of alginate and hyaluronic acid hydrogels[14] and spatially selective induction of contractility of encapsulated cells within gelatin hydrogels.[15] Additionally, some studies reported on generation of 4D constructs with geometries similar to portions of specific target native tissues. For example, 3D printed bi-layered photocurable silk fibroin formed tubular constructs resembling the trachea,[16] and GelMA and polyethylene glycol diacrylate bioinks were printed into constructs that adapted their shape to the curvature of cardiac tissue.[17] However, some of these systems didn't demonstrate biomaterial biodegradability, and none of them demonstrated the capacity to precisely tailor construct 4D shape changes or the time frames in which they occur. Importantly, the highest concentrations of cells incorporated within biodegradable and/or biocompatible 4D materials have been limited to between $0.5 – 10.0 \times 10^6$ cells/mL.[13–17] These concentrations are predominantly orders of magnitude lower than that present during development, in healing processes and in native tissues which may be necessary for engineering tissues[18], and none of these systems achieved condensations with differentiating cells within their materials.

To address the aforementioned challenges with current 4D systems, we aimed to engineer a new 4D biomaterial platform endowed with the capacity to undergo tailored geometric changes over time while simultaneously permitting the incorporation of high densities of cells with maintained viability and functionality. To accomplish this, oxidized and methacrylated alginates (OMA) with different degrees of oxidized and methacrylated gelatin (GelMA) were synthesized to form the basis of bi-layered hydrogels by attaching OMA and GelMA hydrogels via simple sequential crosslinking mediated by ultraviolet (UV) irradiation. We hypothesized temporal differences in swelling rates between the two materials would drive structural deformations. Specifically, it was examined whether higher oxidation of OMA hydrogels would lead to greater swelling and shape change over time compared to the adjacent GelMA hydrogels, which possess relatively lower swelling

properties. The roles of layer thickness, controlled by varying the thickness of spacers between glass plate molds, and the density of incorporated cells [i.e., NIH3T3 fibroblasts and human adipose tissue-derived stromal cells (ASCs)], on the system's 4D characteristics were also evaluated. NIH3T3 and ASCs were then incorporated into the 4D constructs at high densities of ~ 1.0×10^8 cells/mL to determine the capacity for the system to maintain high cell viability. Organization and function of the high cell density constructs were assessed by investigating cell-cell and cell-ECM interactions and differentiation capabilities. Lastly, the feasibility of using the two cell-laden polymer components as bioink materials for bioprinting 4D high cell density constructs with complex initial and pre-programmed final geometries was explored. This study presents a new, versatile 4D high cell density tissue condensation system based on biodegradable and cytocompatible materials enabling precise control of geometric change over time and development of functional 4D tissue constructs.

Results and Discussion

4D tissue engineering maybe a promising technology to partially recapitulate the controlled, programmed geometric reorganization of developing and healing tissues while synchronizing with growth and shape changes of surrounding tissues. By recreating the spatiotemporal changes during native development and repair processes, it also may find utility in the development of artificial tissue models for drug screening.[4] In this study, we exploited differential swelling of oxidized and methacrylated alginate (OMA) and methacrylated gelatin (GelMA), which are widely used biocompatible, biodegradable hydrogel materials, to form constructs that can change their geometry over time when placed in aqueous solutions.[19–22] Importantly, 4D high cell density constructs were fabricated by incorporating cells into the photocrosslinkable OMA/GelMA hydrogels at high densities of up to 1.0×10^8 cells/mL. Bi-layered OMA/GelMA hydrogel constructs were prepared via sequential photocrosslinking (Figure. 1a). Rectangular shaped punches of the hydrogels were used as model constructs to assess 4D spatiotemporal geometric changes over time. We hypothesized that the OMA layer could be designed to exhibit greater swelling than the GelMA layer, and thus drive construct shape changes, due to its greater expansion by water absorption and easily tunable degradation rate. The degree of expansion of the OMA layer was controlled by extent of theoretical oxidation.[19] Additionally, the effects of hydrogel layer thickness, macromer concentration, and density of incorporated cells on the degree of shape change of the model constructs were assessed, and ultimately fabrication of 4D high cell density tissues with defined spatiotemporal geometric change properties were evaluated.

^{1}H-NMR analysis was performed to characterize the OMA and GelMA macromer materials. It was determined that the 15% oxidized OMA (OMA15) exhibited greater intensity at 5.5 ppm compared to the 10% oxidized OMA (OMA10), indicating control over alginate oxidation rate (Figure. 1b).[19] Efficient methacrylation of the OMA and GelMA (Figure. 1c) was demonstrated by recognizable peaks labeled as M (OMA at 6.2, 5.7 and 1.9 ppm, GelMA 5.6, 5.4 and 1.9 ppm)[19, 23], with actual MA rates of OMA10, OMA15 and GelMA being 10.1, 12.5 and 97.4 %, respectively. The swelling ratios of OMA10, OMA15 and GelMA hydrogels were then measured over time (Figure. 1d). At the same macromer concentration of 12%, OMA15 hydrogels presented the highest swelling ratio, 18.7 ± 0.5, at 14 days of incubation and then dramatically decreased at 21 days due to rapid degradation

(Figure. 1e). 12%OMA10 and 12%GelMA presented similar values through 7 days, but 12%OMA10 exhibited greater values at 14 and 21 days (15.2 ± 0.6 and 15.4 ± 0.6) than those of 12%GelMA. The 15%GelMA hydrogel presented the lowest values for all time points except at 21 days. To measure degradability in serum containing high glucose Dulbecco's Modified Eagle's Medium (HG-DMEM) over time, the mass loss of the hydrogels was measured. OMA hydrogels displayed significantly faster degradation than the GelMA hydrogels. OMA15 presented similar mass loss as OMA10 after 7 days, and then underwent more rapid degradation by days 14 to 21 with values of 60.6 ± 10.2 and 95.3 ± 6.5 % respectively. This finding supports the more rapid and extensive swelling observed with the OMA15 compared to the OMA10. However, repeated lyophilization and manipulation of the hydrogels while measuring weight may have played a role in accelerating the mass loss of the OMA15 hydrogels. The GelMA hydrogels exhibited minimal degradation after 14 days, and then gradually lost mass by 21 days. Oxidation cleaves C-C bonds of the *cis*-diol groups of the alginate uronate residues and converts them to dialdehyde groups, making the alginate more susceptible to degradation via hydrolysis. Ester bonds generated by photocrosslinking of the methacrylated polymers are hydrolysable as well.[19] Although GelMA exhibits little degradation in DMEM, its degradation can be accelerated by incorporation of cells due to proteolysis mediated by cell-secreted MMPs.[24] Since it was anticipated that increased shape change would occur in hydrogel bi-layers with greater differences in swelling ratios between the OMA and GelMA, bi-layers of 12%OMA15 and 15%GelMA were expected to exhibit the most extensive change in shape of the conditions examined.

Bi-layered OMA/GelMA hydrogels were fabricated by sequential photocrosslinking to determine the effect of swelling ratio on degree of shape change by observing rectangular hydrogels (width: 2.8 mm, length: 12.7 mm and thickness: 0.4 mm (OMA 0.2 mm + GelMA 0.2 mm)) incubated in NIH3T3 fibroblast culture media for 21 days at 37 °C. Shape change was quantified by measuring of the angle between two lines respectively drawn from bird's-eye view (Figure. S1a) by connecting the center point of the longest dimension of the construct and each end point of the construct. Briefly, a higher value indicates greater shape change with a flat construct in its original shape having an angle of 0°, a construct forming a closed circle measuring at 180°, and a rolled structure where the end points pass each other having a > 180° value (Figure. S1b). All the hydrogels were flat at day 0 and curved into a "C" shape or rolled structure overtime (Figure. 2a and 2b). As hypothesized, hydrogels composed of an OMA15 layer exhibited greater degrees of shape change when compared to those containing OMA10. Interestingly, the 12%OMA15/12%GelMA and 12%OMA15/15%GelMA constructs both rapidly attained a rolled structure by 7 days. However, only the 12%OMA15/12%GelMA maintained the rolled structure through 21 days (239 ± 3°). 8%OMA15/12% and 15%GelMA constructs were also examined, but the 8%OMA15 constructs were unable to undergo strong shape changes, possibly due to decreased water absorption as compared to the 12%OMA15 (Figure. S2a). The effects of increasing the thickness of either the OMA or GelMA layer in the 12%OMA15/12%GelMA constructs was then investigated. Total thickness of bi-layered constructs was set to 0.6 mm, while thicknesses of OMA/GelMA were varied as 0.2/0.4 mm and 0.4/0.2 mm respectively through the use of spacers. It was observed that a 0.4 mm OMA layer induced greater shape

change as compare to a 0.2 mm OMA layer (Figure. 2c). Remarkably, an increase in OMA thickness from 0.2 to 0.4 mm resulted in continuously increasing shape change over 21 days, reaching a curvature of 306 ± 1° (Figure. 2d). Conversely, decreasing OMA thickness to 0.2 mm while increasing the GelMA thickness to 0.4 mm induced minimal geometric change after 7 days, which was not maintained beyond this time point. Therefore, by varying the design parameters (i.e., macromer concentration, degree of alginate oxidation, and layer thickness) of degradable bi-layered OMA/GelMA constructs with potential for high cell density encapsulation and condensation, we have gained an understanding of the underlying principles that regulate their 4D geometric change. Exquisite control of these shape changes over a wide range of deformations may enable mimicry of varied tissue structures from the gentle the curvature of the cornea to the coiled cochlea.

Although studies regarding 4D biomaterials accompanied with cell encapsulation have reported time dependent shape change[25], they have been limited in immediate or very short term geometric changes. For example, in the case of alginate and hyaluronic acid hydrogels with gradient crosslinking[14] and bi-layered PEG hydrogels [13], focus was only on the time scale of seconds and minutes without precise temporal control over 4D shape changes on the time scale of days and weeks that is required for healing and development processes of tissue[26] and that can be achieved with the OMA/GelMA system. In addition, there has not previously been a system that permits encapsulation of a high density of viable cells in biocompatible and biodegradable materials with pre-designed geometric changes over time. It was expected that the bi-layered constructs composed of cell friendly, biodegradable OMA/GelMA[19–21] would enable cells to be incorporated at a high density. The shape-changing feature of the cell containing 4D biodegradable constructs was not anticipated to be affected by the high cell density encapsulation. The GelMA, synthesized from gelatin that is denatured collagen and has important biochemical functionality[22], was anticipated to provide a favorable environment to the incorporated cells by presenting cell adhesive moieties that are not present in non-degradable synthetic polymers.[27] To assess the ability to incorporate high cell density concentrations without affecting subsequent 4D geometric changes, NIH3T3 cells were incorporated in a 12%GelMA layer with varied densities of 2.0, 5.0×10^7, and 1.0×10^8 cells/mL. A 0.2 mm layer of 12%OMA15 hydrogel was used to induce geometric change. Increase in the cell density could be visualized using phase contrast microscopy from a side view (Figure. S3a). For the 1.0×10^8 cells/mL condition, a 0.4 mm of OMA15 layer was additionally applied in efforts to induce slow but longer lasting shape change for long term culture periods (Figure 3a). As quantified in Figure. 3b, the 2.0 and 5.0×10^7 cells/mL conditions showed more extensive geometric changes than 1.0×10^8 cells/mL condition at 3 and 7 days with statistical significance, but lower cell concentration conditions were unable to maintain their maximal rolled structures at 21 days. Interestingly, the 1.0×10^8 cells/mL condition with a thinner OMA layer exhibited a slower shape change profile but steadily increased and maintained the rolled structure until 21 days (221 ± 6°) (Figure. 3b). The highest cell density with a thicker OMA layer displayed slower shape changes, but also successfully induced a rolled structure similar to that of its thinner construct counterpart during 21 days of culture (213 ± 5°). To the best of our knowledge, 1.0×10^8 cells/mL is the highest density to ever be reported in a shape changing material, which is 20 times greater than the highest previous reported concentration, 5.0×10^6 cells/mL.[14]

It may not be possible to incorporate higher concentrations of cells in systems that rely on gradient crosslinking through light irradiation as the increase in cell density in the macromer solutions can inhibit light penetration and hinder gradient crosslinking generation. The ability to use a wide range of cell densities shown in this study is beneficial for engineering different target tissues that have varied cell concentrations. A DNA assay conducted on samples from the 1.0×10^8 cells/mL and 0.4 mm OMA layer condition revealed maintenance of DNA content, approximately 1.2 μg/sample over 21 days, indicating viable cells within the constructs (Figure. 3c). Live/Dead stained images of the constructs obtained at 1 and 21 days showed predominantly live (green) fluorescence evidence of high cell viability in the 4D constructs (Figure. 3d).

ASCs were then incorporated into the constructs at a density of 1.0×10^8 cells/mL into a 0.2 mm 12%GelMA layer and 0.4 mm 12%OMA15 was additionally layered. To assess potential to drive cellular differentiation simultaneously during the induction of 4D material shape change, the samples were incubated in 3 different media: growth, chondrogenic and osteogenic (Figure. 3e). Similar to the NIH3T3 cells, it was observed that every group presented steady increases in degree of geometric change after 3 days of culture (Figure. 3f). Samples cultured in control growth media formed a closed circle, while the experimental groups formed even more fully rolled structures beyond a complete circle by 21 days (232 ± 7° and 212 ± 5° for osteogenic and chondrogenic differentiation conditions, respectively). The incorporated ASCs presented high viability regardless of culture condition or time period (Figure. S4). DNA content of the constructs presented similar levels without significant differences, near 1.0 μg/sample (Figure. 3g). However, significant increases in GAG/DNA and ALP activity/DNA were observed between the growth media condition and chondrogenic and osteogenic differentiation media conditions, respectively (Figure. 3h and 3i). Positive histologic staining for GAG production and calcium deposition in the samples cultured in differentiation media corroborated the biochemical findings, demonstrating the capacity to differentiate encapsulated stem cells down specific connective tissue lineages in the 4D material while also achieving controlled changes in construct shape (Figure. 3j and 3k). Previous reports with encapsulated cells in biodegradable 4D materials have mainly investigated geometric changes without focusing on cellular behaviors. In this study, a range of cellular activities and functions have been investigated, including viability, proliferation, and differentiation.

To demonstrate the potential to generate high cell density 4D tissue constructs comprised of two physically separated cell populations, NIH3T3 cells were further incorporated into both the GelMA and OMA15 layers (cell density = 1×10^8 cells/mL), 12%OMA15 with 0.4 mm thickness and 12%GelMA with 0.2 mm thickness. It was clearly apparent that the cells were incorporated into both layers of the high cell density 4D constructs via phase contrast and fluorescence imaging (Figure. 4a), and H&E staining (Figure S5a). NIH3T3 cells labeled with violet and green dyes and incorporated in GelMA and OMA layers, respectively, can be seen in their respective layers in fluorescence photomicrographs. Incorporation of at least two different cell types in separate distinct compartments is also possible via this sequential bilayer crosslinking system, which is not achievable in platforms relying on gradient crosslinking of a single component.[14] This capability may be advantageous in efforts toward building 4D high cell density constructs recapitulating complex native tissues

composed of multiple cell types. The dual cell incorporated samples presented a similar degree of geometric change (232 ± 10°) at 14 days (Figure. 4b and 4c) compared to 4D materials containing cells only in the GelMA layer at a density of 1×10^8 cells/mL (Figure. 3a and 3b).

To investigate additional capacity to further control 4D construct shape change via photolithography[13, 28, 29], an OMA layer comprised of evenly spaced 250 μm wide strips (Figure. 4d) “parallel” or “perpendicular” to the longest dimension of the model construct was selectively added to the GelMA layer using a photomask. Generation of shape-morphing 12%OMA15/12%GelMA (0.2 mm/0.2 mm in thickness) bi-layered regions with different directionality of the OMA strips was expected to control degree of the self-rolling. The perpendicular pattern group showed rapid rolling immediately after the fabrication (at 0 day) and formed and maintained a ‘C’ shape over 7 days of culture (Figure. 4e). The parallel pattern group exhibited less shape change immediately after fabrication (at 0 day) and presented a different time course of curved structure formation from that of perpendicular pattern group, but also underwent geometric change into a ‘C’ shape. These results highlight additional system capabilities for guided geometric shape change by simple application of photomasks with varied patterns and directions.

Lastly, the capabilities of the system performance were investigated in conjunction with bioprinting constructs possessing more complex structures using a 3D bio-printer (Figure. 4f and 4g). To demonstrate capacity to simultaneously modulate multiple bioprinting system parameters such as type of ink material and cell density, cells were incorporated at densities of 1.0×10^8 and 1.0×10^7 cells/mL in the 12%OMA15 and 12%GelMA solutions, respectively. The inks were printed by adapting the free form reversible embedding of suspended hydrogels (FRESH) technique using a multi-nozzle printer with assistance of a gelatin microgel slurry bath.[30] This printing system was used to produce a 2×2 bilayered checkerboard construct with total dimensions of 2 cm × 2 cm × 0.4 cm. Each small cube of the cell-laden OMA and cell-laden GelMA, indicated with red and white, respectively, in Figure. 4f, has a dimension of 1 cm × 1 cm × 0.2 cm. After removing the gelatin slurry by incubating at 37 °C for 1 hr, the printed 4D construct reflected the original CAD file (Figure. 4g). Although the cube did not show any curved or angular structures at the borders of the OMA and GelMA regions in the checkerboard pattern at 0 day, after 7 days the cultured construct exhibited slight curvature in these areas as indicated with white dashed lines. Patterning cell-laden inks with different swelling ratio in this system has great potential for creating 4D high cell density constructs with complicated structural hierarchy. To our best knowledge, this is the first study demonstrating successful printing of cytocompatible and biodegradable 4D constructs containing cells in high density to achieve controlled geometric shape changes by thoughtful design and selection of the system parameters.

3. Conclusion

In summary, we have developed novel 4D high cell density constructs which undergo controlled temporal changes in geometry that are regulated by tailored spatial patterning of biodegradable OMA and GelMA materials with differential swelling ratios. By exploiting the simple model construct of bi-layered OMA/GelMA hydrogels, it was demonstrated that

higher oxidation extent of the OMA, which increases its degradation rate and swelling, facilitates greater geometric shape changes. Multiple construct parameters such as macromer percentage, layer thickness, cell density and patterns generated by photolithography were varied to precisely program the final geometry of the 4D construct. In addition, high cell density encapsulation in biomaterial-based 4D constructs (1.0×10^8 cells/mL) was achieved to mimic cellular condensations in native tissues. This technique supported normal cellular activities such as differentiation down towards osteogenic and chondrogenic lineages with minimal apparent adverse effects on viability. The photocrosslinking-based system permits building of complex tissues with multiple cellular components via specific spatial placement of different cell types. Bioprinting the cell-laden OMA and GelMA inks confirmed the ability to print 4D responsive high cell density constructs with complex geometries. Importantly, this strategy may be more broadly applied using other commonly used biodegradable materials with differential swelling ratios. This study presents a paradigm changing platform technology that has the potential to significantly impact 4D tissue engineered therapeutics for treatment of damaged tissues, investigation of questions in developmental biology, and formation of tissue models for drug testing.

Experimental section

Synthesis of OMA and GelMA:

To synthesize OMA, 1% sodium alginate (10 g, Protanal LF 20/40, FMC Biopolymer) solution was dissolved in ultrapure deionized water (diH_2O, 900 ml) by stirring overnight at room temperature (RT). Either 1 or 1.5 g of sodium periodate were respectively dissolved in 100 ml of diH_2O, mixed with the alginate solution to achieve 10% and 15% theoretical alginate oxidation and reacted in the dark at RT for 24 hrs under stirring. 2-morpholinoethanesulfonic acid (MES, 19.52 g, Sigma) and NaCl (17.53 g) were then dissolved in the oxidized alginate solution and the pH was adjusted to 6.5 using 4 N NaOH. N-hydroxysuccinimide (NHS, 1.176 g, Sigma) and 1-ethyl-3-(3-dimethylaminopropyl)-carbodiimide hydrochloride (EDC, 3.888 g, Sigma) were dissolved into the mixture. AEMA (1.688 g, Polysciences) (molar ratio of NHS:EDC:AEMA = 1:2:1) was then slowly added to the solution to achieve a theoretical methacrylation level of 20%. The reaction was conducted at RT for 24 hrs in the dark. The reacted OMA solution then was poured into excess acetone to precipitate the OMA. The precipitate was dried in a fume hood and subsequently dissolved in diH_2O at a 1% w/v concentration. The OMA solution was dialyzed for purification using a dialysis membrane (MWCO 3500, Spectrum Laboratories Inc.) for 3 days. The dialyzed OMA solution was collected and treated with activated charcoal (5 g/L, 50–200 mesh, Fisher) for 30 min. The solution was further purified and sterilized by filtering through a 0.22 μm pore membrane and then lyophilized.

To synthesize GelMA, 10 g of gelatin (type A, Sigma Aldrich) was dissolved in 100 ml of PBS (pH 7.4) and heated to 50 °C. Then 10 ml of methacrylic anhydride was added into the 10% gelatin solution and reacted for 1 hr at 50 °C and then stirred overnight at RT. GelMA was precipitated with acetone, purified via dialysis at 50 °C for 7 days with a MWCO 12–14k membrane (Spectrum Laboratories Inc.), sterilized via a 0.22 mm pore filter, and then lyophilized. To obtain ^{1}H-NMR spectra, the OMA and GelMA were separately dissolved in

deuterium oxide (D_2O) at 2 w/v % and the samples were analyzed via ^{1}H-NMR spectrometer (Varian Unity-300 (300MHz) NMR spectrometer (Varian Inc.)). 3-(trimethylsilyl)propionic acid-d_4 sodium salt (0.05 w/v %) was used as an internal standard. The actual methacrylation of the OMA and GelMA was determined from ^{1}H NMR spectra based on the ratio of the integrals for the internal standard protons to the methyl and methylene protons of methacrylate (indicated as M, Figure 1b and 1c).

Cell isolation and expansion culture:

NIH3T3s were cultured and in NIH3T3 growth medium (10% FBS, 1% PS in HG-DMEM). ASCs were obtained from the adipose tissue using a previously reported method.[31] Briefly, lipoaspirates were treated with 200 U/mg collagenase type I (Worthington Biochemical Products, Lakewood, NJ) digestion for 40 min at 37 °C. The stromal fraction was then isolated though centrifugation and plated and cultured on tissue culture plastic (TCP) in DMEM/nutrient mixture F12 (DMEM/F12, BioWhittaker, Suwance, GA) with 10% defined fetal bovine serum (FBS, HyClone, Logan, UT), 100 U/ml penicillin and 100 mg/ml streptomycin (1% P/S, BioWhittaker). Cell culture was conducted under standard conditions (95% humidity, 5% CO_2, 37 °C). The medium was changed every 2 days. Cells were detached from TCP using 0.05% of trypsin/EDTA for passage and experimentation. Passage 3 ASCs were used in this study.

Fabrication of bi-layered OMA/GelMA hydrogel as a model construct:

OMA and GelMA were separately dissolved at multiple different concentrations in HG-DMEM containing 0.05% photoinitiator (PI, Irgacure-2959). For cell incorporation, NIH3T3s or ASCs were collected via standard trypsinization, and pre-determined numbers of cells were collected after cell counting and centrifugation. Cell pellets were dissociated into OMA or GelMA solutions at designated densities of 2.0×10^7, 5.0×10^7 and/or 1.0×10^8 cells/ml. The OMA solution (with or without cells) was first cured under UV light (320–500 nm, EXFO OmniCure S1000–1B, Lumen Dynamics Group, Mississauga, Ontario, Canada) at 20 mW/cm^2 for 45 sec between hydrophobic glass plates treated with Sigmacote (Sigma Aldrich) separated with 0.2 or 0.4 mm thick spacers. GelMA solution was then cured under UV at 20 mW/cm^2 for 45 sec on top of the OMA hydrogel between glass plates with 0.6 or 0.8 mm gaps controlled by assembling 0.2 mm spacers. The dual-layered hydrogel was punched into rectangular shapes (width = 2.8 mm, length = 12.7 mm). To generate OMA patterns in the 4D constructs, GelMA was cured first by UV irradiation then OMA was selectively cured later using a photomask.

Culture of cell-laden 4D constructs:

4D constructs containing NIH3T3s were cultured in NIH3T3 growth media. 4D constructs containing ASCs were cultured in ASC growth media or differentiation media. Chondrogenic differentiation of 4D ASC constructs was conducted in a media composed of 1% ITS+ Premix (Corning), 100 nM dexamethasone (MP Biomedicals), 37.5 μg/ml L-ascorbic acid-2-phosphate (Wako USA), 1 mM sodium pyruvate (Hyclone), 100 μM nonessential amino acids (Hyclone), and 10 ng/ml TGF-β1 (Peprotech) in DMEM-high glucose. For osteogenic differentiation, 10 mM β-glycerophosphate (CalBiochem), 50 mM

ascorbic acid (Wako USA), 100 nM dexamethasone (MP Biomedicals), and 100 ng/ml BMP-2 (Perkin-Elmer) in DMEM-high glucose containing 10% FBS and 1% PS was used.

Angle measurement of 4D model constructs:

Photographic images (Galaxy Note 10, Samsung, South Korea) of the model constructs were obtained at different time points. Using Image J software, the center and two end points were determined from a bird's-eye view (Figure. S1a) and two lines starting from the center extending to each end were drawn (Figure. S1b). The angle between the two lines was measured to determine degree of the geometric change. For example, 0° indicates no shape change, 180° denotes a closed circle, and negative values imply a rolled structure beyond a complete circle.

Swelling ratio and degradation test of the OMA and GelMA hydrogels:

Hydrogels were fabricated into the shape of 0.8 mm diameter, 0.75 mm thick discs by placing polymer solution between a quartz and regular glass plate separated by spaces and crosslinking through the quartz plate via UV light at 20 mW/cm^2 for 45 sec and using a biopsy punch. The samples were lyophilized to obtain their initial dry weights (Wi). The lyophilized samples were then immersed in HG-DMEM containing 10 % FBS and 1 % PS and incubated at 37 °C. The media was replaced every other day. Weight of the swollen hydrogels was measured (Ws) and used to calculate the swelling ratio Ws/Wi (n = 4) for each condition per time point. After the measurement, the samples were lyophilized to obtain dry weight (Wd). Mass loss was quantified as (Wi-Wd)/Wi × 100 (n = 3) for each condition per time point.

Live/Dead staining:

Cell-laden 4D constructs were treated with Live/Dead staining solution (0.1% Calcein AM and 0.2% Propidium Iodide in PBS) for 15 min. Fluorescence images were obtained via an ImageXpress PICO (Molecular Devices, CA, USA) with 40X magnification.

Biochemical assays:

4D high cell density constructs were digested in 1 ml papain buffer solution (25 mg/ml papain (Sigma); 2 mM L-cysteine (Sigma); 50 mM sodium phosphate (Sigma); 2 mM ethylenediaminetetraaceticacid (EDTA) (Fisher); pH 6.5 in nuclease-free water (Ambion, Austin, TX) at 65 °C overnight. The samples were then centrifuged at 16200 g for 10 min. 100 µl of supernatant was collected in a 96 well plate then treated with 100 µl of PicoGreen® reagent (Invitrogen, Carlsbad, CA). Fluorescence intensity was then measured on a microplate reader (SpectraMax®, Molecular Devices, CA, USA) at 520 nm (excitation at 480 nm). For GAG quantification, 100 µl of dimethylmethylene blue dye solution was added to 40 µl of the digested supernatant. Absorbance values were measured on the microplate reader at 595 nm. ALP assay was conducted by adding 100 µl of ALP yellow substrate (Sigma) to 100 µl of the digested supernatant. The mixture was incubated at 37 °C for 30 min and then a reaction stop solution (50 µl of 0.1N NaOH) was added. Absorbance at 405 nm was measured on the microplate reader.

Histology:

The 4D high cell density constructs were fixed in 4% neutral buffered formalin and embedded in paraffin. 5 μm thickness sections were loaded on slide glasses. After deparaffinization, sections were stained with Toluidine Blue O or Alizarin Red S for 5 min to visualize GAG and calcium, respectively. For hematoxylin and eosin (H&E) staining, sections were treated with these stains for 10 and 2 min, respectively.

Live cell labeling:

Pre-labeling of NIH3T3 was conducted by treating the cells with 0.5% Vybrant™ DiD (purple fluorescence dye) (Invitrogen) or 0.5% Vybrant™ DiO (green fluorescence dye) (Invitrogen) in culture medium for 1 hr.

3D bioprinting:

The gelatin slurry for supporting bath was prepared as described previously.[30] NIH3T3 laden 12%OMA15 (at 1.0×10^8 cells/ml) and 12%GelMA (at 1.0×10^7 cells/ml) were loaded on separate extruders on a Biobot™ Basic 3D printer (Advanced Solutions Life Sciences, KY, USA) with 1/2 inch stainless metal 25G needles (McMaster-Carr). A gelatin slurry bath filled petri dish was placed on the printer platform, and then a CAD file was used to print a 2×2 bilayered checkerboard construct with total dimensions of 2 cm × 2 cm × 0.4 cm. The printed 4D construct was immersed in HG-DMEM media then moved to a 37 °C incubator to dissolve out the gelatin slurry and further culture in NIH3T3 growth media. After 30 min and 7 days of culture, optical images were obtained using digital camera (Galaxy Note 10, Samsung).

Statistical analysis:

All quantitative data is presented as mean ± standard deviation. Statistical analysis was conducted via one-way analysis of variance (ANOVA) with Tukey significant difference post hoc test using Graphpad Prism 5 software (GraphPad Software, San Diego, CA). A value of $p<0.05$ indicates statistical significance.

Supplementary Material

Refer to Web version on PubMed Central for supplementary material.

Acknowledgements

The authors gratefully acknowledge funding from the National Institutes of Health's National Institute of Arthritis and Musculoskeletal and Skin Diseases (R01AR069564, and R01AR066193; EA), and National Institute of Biomedical Imaging and Bioengineering (R01EB023907; EA). The contents of this publication are solely the responsibility of the authors and do not necessarily represent the official views of the National Institutes of Health.

References

[1]. Bassel GW, Stamm P, Mosca G, Barbier de Reuille P, Gibbs DJ, Winter R, Janka A, Holdsworth MJ, Smith RS, Proceedings of the National Academy of Sciences of the United States of America 2014, 111, 8685. [PubMed: 24912195]

[2]. Stevens KR, Scull MA, Ramanan V, Fortin CL, Chaturvedi RR, Knouse KA, Xiao JW, Fung C, Mirabella T, Chen AX, McCue MG, Yang MT, Fleming HE, Chung K, de Jong YP, Chen CS, Rice CM, Bhatia SN, Science translational medicine 2017, 9.

[3]. Hu JC, Athanasiou KA, Tissue engineering 2006, 12, 969. [PubMed: 16674308]

[4]. Gao B, Yang Q, Zhao X, Jin G, Ma Y, Xu F, Trends in biotechnology 2016, 34, 746. [PubMed: 27056447]

[5]. Torras N, Garcia-Diaz M, Fernandez-Majada V, Martinez E, Frontiers in bioengineering and biotechnology 2018, 6, 197. [PubMed: 30619844]

[6]. Senatov FS, Niaza KV, Zadorozhnyy MY, Maksimkin AV, Kaloshkin SD, Estrin YZ, Journal of the mechanical behavior of biomedical materials 2016, 57, 139. [PubMed: 26710259]

[7]. Stroganov V, Zakharchenko S, Sperling E, Meyer AK, Schmidt OG, Ionov L, Adv Funct Mater 2014, 24, 4357.

[8]. Sakar MS, Neal D, Boudou T, Borochin MA, Li Y, Weiss R, Kamm RD, Chen CS, Asada HH, Lab on a chip 2012, 12, 4976. [PubMed: 22976544]

[9]. Luo YX, Lin X, Chen BR, Wei XY, Biofabrication 2019, 11.

[10]. Kokkinis D, Schaffner M, Studart AR, Nature communications 2015, 6.

[11]. Borriello A, Guarino V, Schiavo L, Alvarez-Perez MA, Ambrosio L, J Mater Sci-Mater M 2011, 22, 1053. [PubMed: 21373812]

[12]. Kuribayashi-Shigetomi K, Onoe H, Takeuchi S, Plos One 2012, 7.

[13]. Jamal M, Kadam SS, Xiao R, Jivan F, Onn TM, Fernandes R, Nguyen TD, Gracias DH, Advanced healthcare materials 2013, 2, 1142. [PubMed: 23386382]

[14]. Kirillova A, Maxson R, Stoychev G, Gomillion CT, Ionov L, Adv Mater 2017, 29, 1703443.

[15]. Miotto M, Gouveia RM, Ionescu AM, Figueiredo F, Hamley IW, Connon CJ, Adv Funct Mater 2019, 29.

[16]. Kim SH, Seo YB, Yeon YK, Lee YJ, Park HS, Sultan MT, Lee JM, Lee JS, Lee OJ, Hong H, Lee H, Ajiteru O, Suh YJ, Song SH, Lee KH, Park CH, Biomaterials 2020, 260, 120281. [PubMed: 32858503]

[17]. Cui H, Liu C, Esworthy T, Huang Y, Yu ZX, Zhou X, San H, Lee SJ, Hann SY, Boehm M, Mohiuddin M, Fisher JP, Zhang LG, Science advances 2020, 6, eabb5067. [PubMed: 32637623]

[18]. Skylar-Scott MA, Uzel SGM, Nam LL, Ahrens JH, Truby RL, Damaraju S, Lewis JA, Science advances 2019, 5, eaaw2459. [PubMed: 31523707]

[19]. Jeon O, Alt DS, Ahmed SM, Alsberg E, Biomaterials 2012, 33, 3503. [PubMed: 22336294]

[20]. Jeon O, Samorezov JE, Alsberg E, Acta biomaterialia 2014, 10, 47. [PubMed: 24035886]

[21]. Jeon O, Wolfson DW, Alsberg E, Adv Mater 2015, 27, 2216. [PubMed: 25708428]

[22]. Samorezov JE, Headley EB, Everett CR, Alsberg E, Journal of biomedical materials research. Part A 2016, 104, 1387. [PubMed: 26822338]

[23]. Jeon O, Powell C, Solorio LD, Krebs MD, Alsberg E, J Control Release 2011, 154, 258. [PubMed: 21745508]

[24]. Tondera C, Hauser S, Kruger-Genge A, Jung F, Neffe AT, Lendlein A, Klopfleisch R, Steinbach J, Neuber C, Pietzsch J, Theranostics 2016, 6, 2114. [PubMed: 27698944]

[25]. Hilderbrand AM, Ovadia EM, Rehmann MS, Kharkar PM, Guo C, Kloxin AM, Current opinion in solid state & materials science 2016, 20, 212. [PubMed: 28717344]

[26]. Vats A, Tolley NS, Polak JM, Gough JE, Clinical otolaryngology and allied sciences 2003, 28, 165. [PubMed: 12755749]

[27]. Lee YB, Lee JY, Byun H, Ahmad T, Akashi M, Matsusaki M, Shin H, Biofabrication 2018, 10.

[28]. Stoychev G, Turcaud S, Dunlop JWC, Ionov L, Adv Funct Mater 2013, 23, 2295.

[29]. Kapyla E, Delgado SM, Kasko AM, ACS Appl Mater Interfaces 2016, 8, 17885. [PubMed: 27322508]

[30]. Hinton TJ, Jallerat Q, Palchesko RN, Park JH, Grodzicki MS, Shue HJ, Ramadan MH, Hudson AR, Feinberg AW, Science advances 2015, 1, e1500758. [PubMed: 26601312]

[31]. Estes BT, Diekman BO, Gimble JM, Guilak F, Nature protocols 2010, 5, 1294. [PubMed: 20595958]

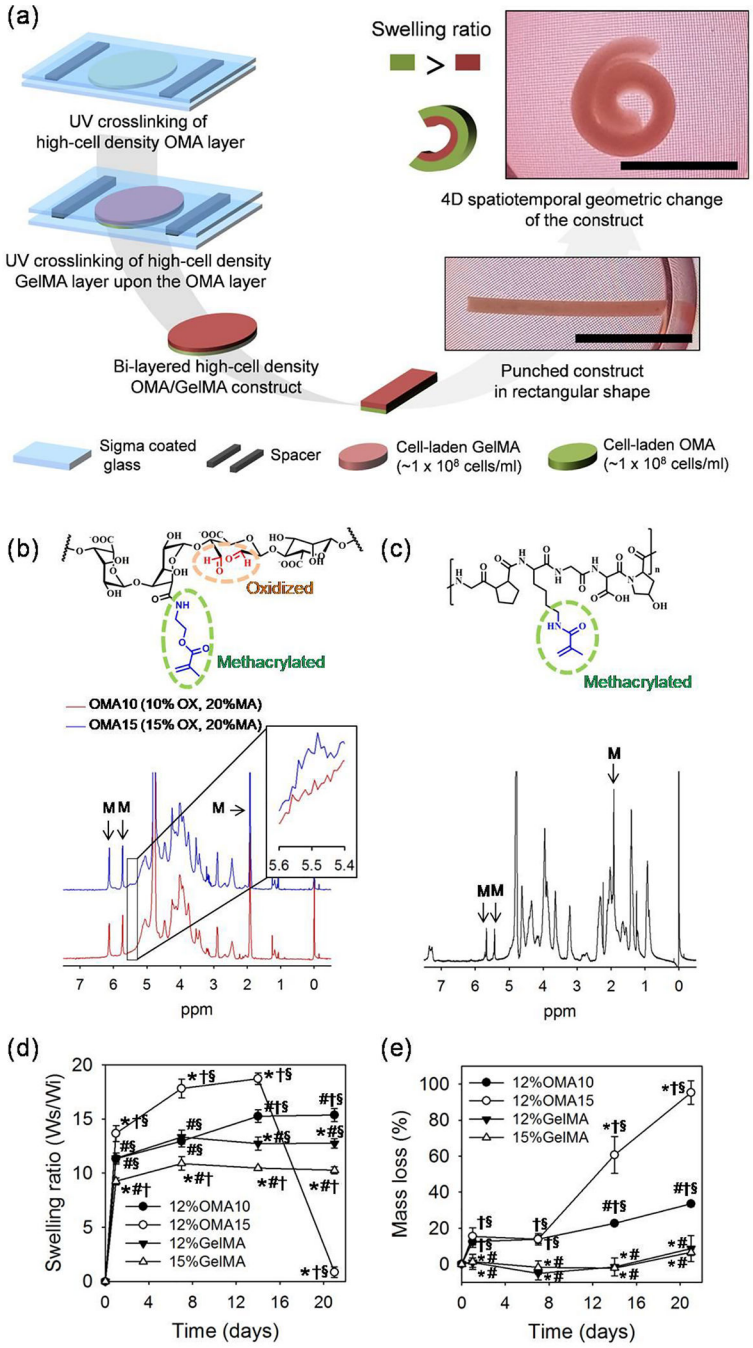

Figure 1.

(a) Schematic diagram for fabricating 4D high cell density model construct based on different swelling ratios between OMA and GelMA. Bi-layered high cell density (0.2 – 1.0 × 10^8 cells/mL) OMA/GelMA constructs spontaneously changed geometry into rolled structures. Scale bars indicate 1 cm. Chemical structures and NMR analysis for (b) the OMA with different theoretical oxidation rates of 10 and 15% with fixed theoretical 20% methacrylation rate and (c) the GelMA. Magnified OMA NMR spectra from 5.4 to 5.6 ppm is presented in a small box on upper right side of the OMA NMR graph. “M” labels indicate

methacrylation peaks of the polymers. Profiles of (d) swelling and (e) degradation of the individual OMA and GelMA hydrogels over 21 days of culture. “*”, “#”, “†” and “§” indicate statistical significance compared to 12%OMA10, 12%OMA15, 12%GelMA and 15%GelMA, respectively ($p < 0.05$).

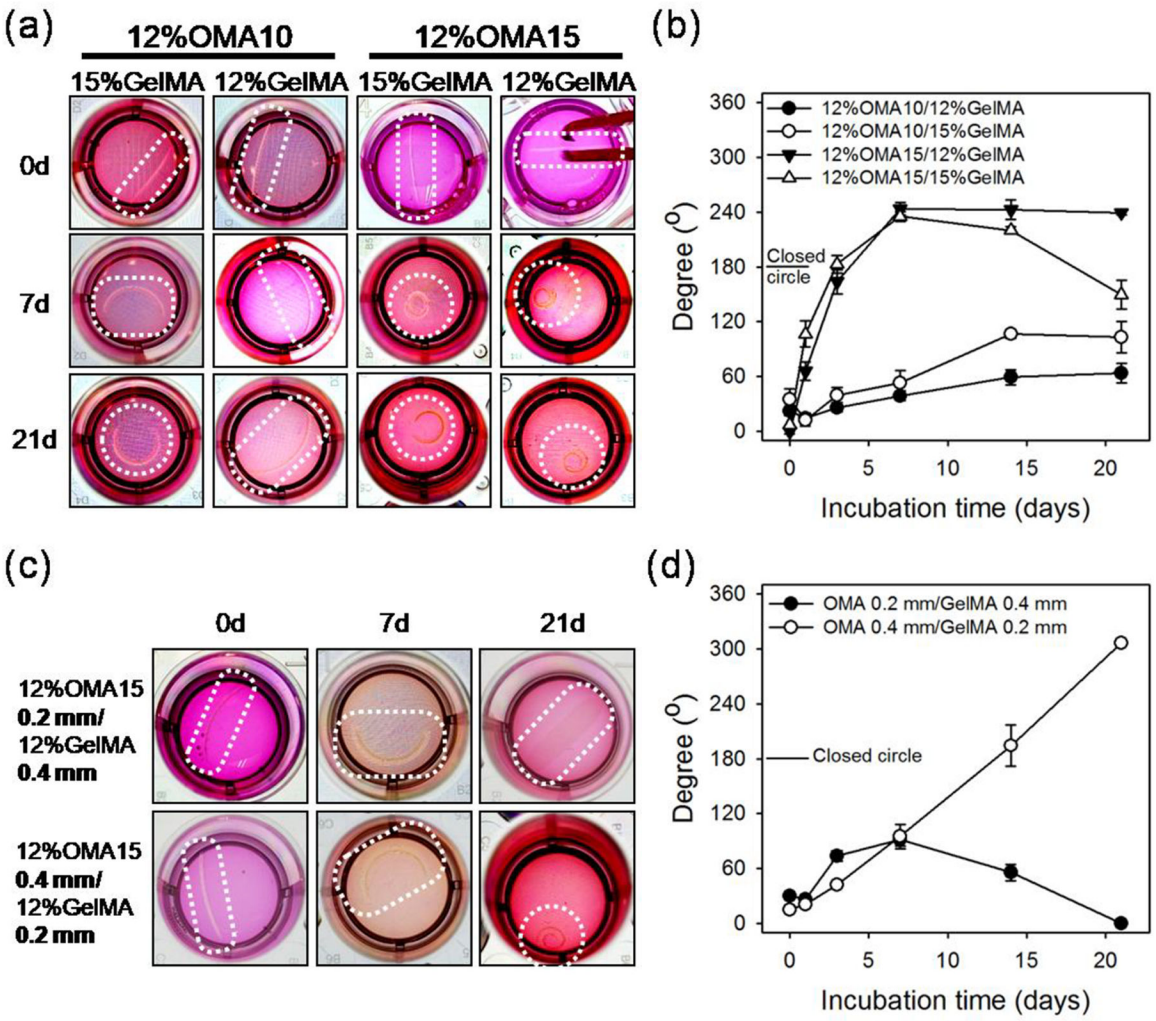

Figure 2.

(a) Photographic images and (b) angle measurements of the bended or rolled model 4D constructs demonstrating the effect of OMA oxidation rate and macromer percentages of GelMA on 4D geometric changes. Diameter of the wells is 15.6 mm. (c) Photographic images and (d) angle measurements of the bended or rolled model 4D constructs with varied thickness ratios of OMA and GelMA layers at fixed overall construct thickness of 0.6 mm demonstrating the effect of layer thicknesses on 4D geometric changes. Diameter of the wells is 15.6 mm.

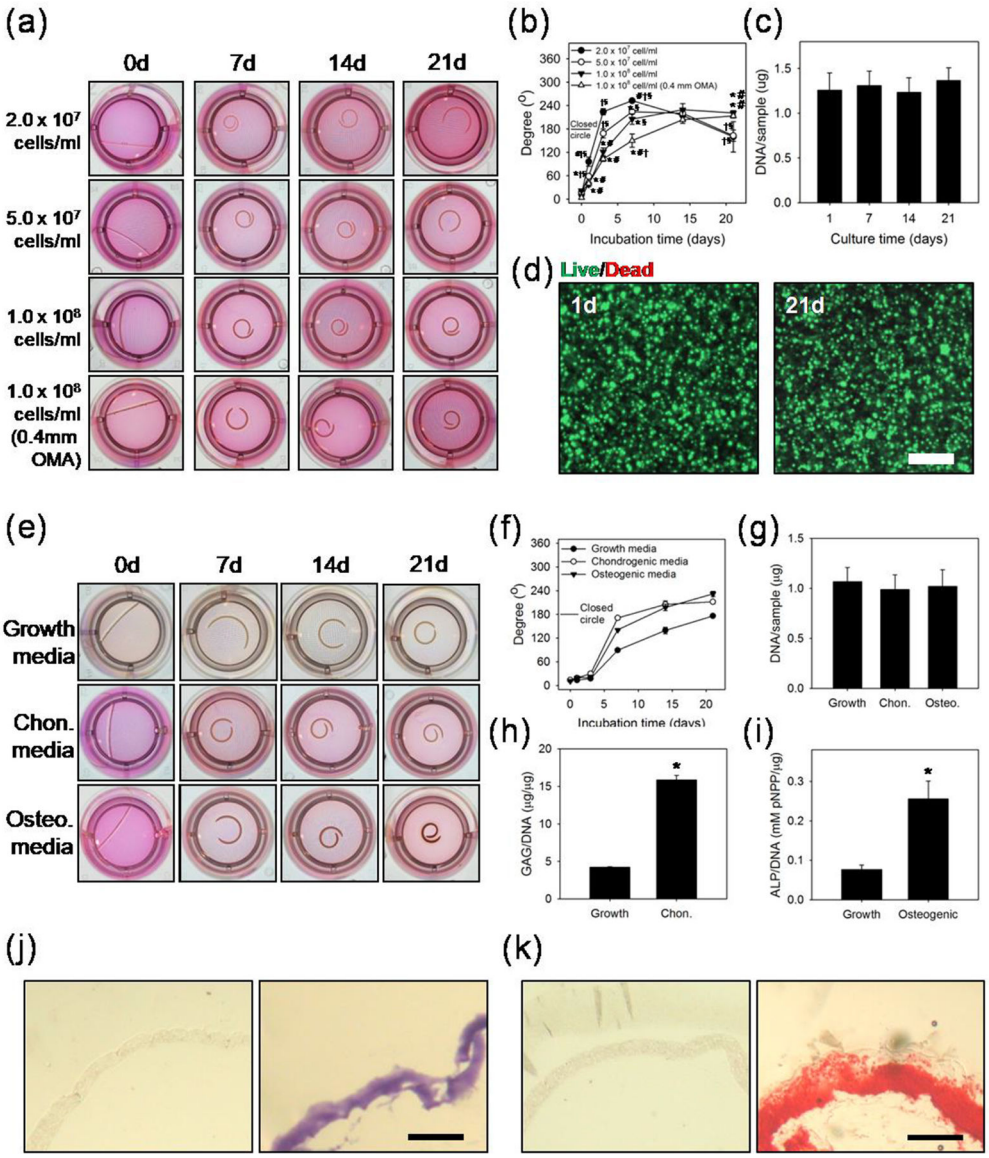

Figure.3.

(a) Photographic images and (b) angle measurements of the bended or rolled model 4D constructs containing NIH3T3 cells in the GelMA layer to determine the effect of cell density and OMA layer thickness on the 4D geometric change. Diameter of the wells is 15.6 mm. “*”, “#”, “†” and “§” indicate statistical significance compared to 2.0×10^7 cells/mL, 5.0×10^7 cells/mL, 1.0×10^8 cells/mL and 1.0×10^8 cells/mL with 0.4 mm OMA groups, respectively. (c) DNA content of the 4D high cell density constructs with 1.0×10^8 cells/mL and 0.4 mm OMA thickness at different time points. (d) Live/dead stained images of the high cell density construct at 1 and 21 days of culture. Scale bar indicates 200 μm. (e) Photographic images of the bent or rolled model 4D constructs containing ASCs in the GelMA layer at 1.0×10^8 cells/mL density which were cultured in growth, chondrogenic or osteogenic differentiation media over 21 days to demonstrate differentiation capacity in the system and (f) angle measurement of the bent or rolled model ASC 4D constructs. Diameter

of the wells is 15.6 mm. (g) DNA content of the 4D ASC constructs cultured in the different media for 21 days. (h) GAG production/DNA of 4D ASC constructs cultured in chondrogenic and growth media for 21 days. (i) ALP activity/DNA of 4D ASC constructs cultured in osteogenic and growth media for 21 days. "*" indicates significant statistical difference ($p < 0.05$). Cross-sectional images of (j) Toluidine Blue O stained sections of control group cultured in growth media (left) and chondrogenically differentiated 4D ASC construct demonstrating GAG production (right). (k) Alizarin Red S stained sections of control group cultured in growth media (left) and osteogenically differentiated 4D ASC construct demonstrating calcium deposition (right). Scale bars in (j) and (k) indicate 1 mm.

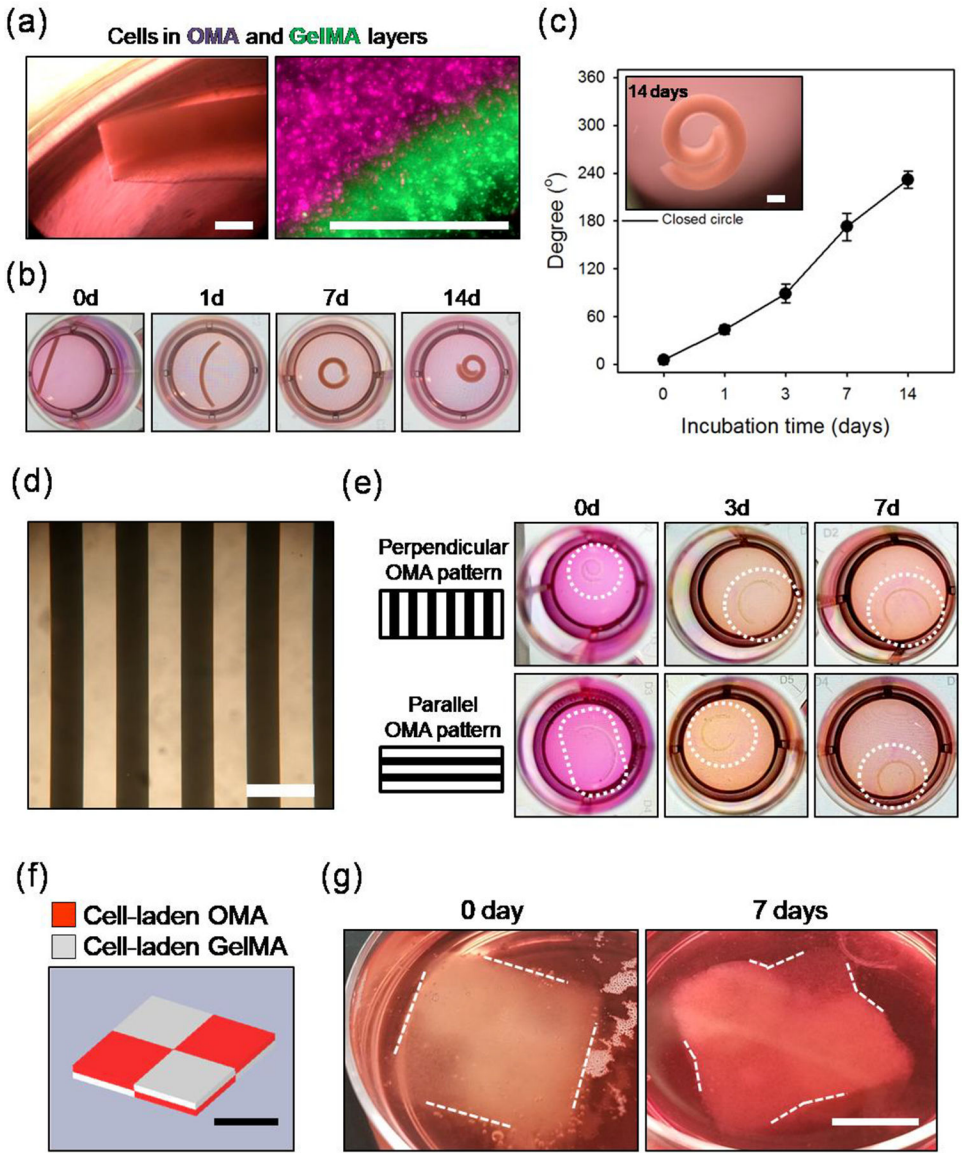

Figure.4.

(a)Photographic images over 14 days of 4D high cell density constructs composed of 0.2 mm cell-laden GelMA and 0.4 mm cell laden-OMA layers. NIH3T3 cells were incorporated at 1.0×10^8 cells/mL in both layers. The diameter of the wells in the images is 15.6 mm. (b) Images exhibiting the presence of NIH3T3 cells in both the GelMA and OMA layers. Left image is a phase contrast image of the construct and right image is a fluorescence image of cells labeled with purple and green dyes in the 12%OMA15 and 12%GelMA layers, respectfully. Scale bars indicate 500 μm. (c) Angle measurements of the 4D high density NIH3T3 (1.0×10^8 cells/ml) constructs during 14 days of culture and image of the construct at 14 days (scale bar = 1 mm). (d) Photographic image of a photomask used to generate a pattern of alternating regions of photocrosslinked OMA in the model construct. Scale bar indicates 500 μm. (e) Photographic images of the bent constructs over 7 days corresponding to OMA pattern directions perpendicular or parallel to the constructs' longest axis. Diameter

of the wells is 15.6 mm. (f) CAD image of layered checkerboard pattern. Red and light gray indicate cell-laden OMA and GelMA regions, respectively. (g) 4D high cell density layered checkerboard construct fabricated by printing NIH3T3-laden 12%OMA15 (1.0×10^8 cells/mL) and NIH3T3-laden 12%GelMA (1.0×10^7 cells/mL) inks using a CAD file. The printed construct was flat and did not exhibit curvature or angled shape at day 0, while defined 4D geometric changes occurred over the course of 7 days culture as indicated by white dotted lines. Scale bars in (f) and (g) indicate 1 cm.